Defects, Disorder, and Strong Electron Correlations in Orbital Degenerate, Doped Mott Insulators

Adolfo Avella,[1,2,3] Andrzej M. Oleś,[4,5] and Peter Horsch[4]
[1]Dipartimento di Fisica "E.R. Caianiello," Università degli Studi di Salerno, I-84084 Fisciano (SA), Italy
[2]CNR-SPIN, UoS di Salerno, I-84084 Fisciano (SA), Italy
[3]Unità CNISM di Salerno, Università degli Studi di Salerno, I-84084 Fisciano (SA), Italy
[4]Max-Planck-Institut für Festkörperforschung, Heisenbergstrasse 1, D-70569 Stuttgart, Germany
[5]Marian Smoluchowski Institute of Physics, Jagiellonian University, prof. Łojasiewicza 11, PL-30348 Kraków, Poland
(Received 20 August 2015; published 11 November 2015)

We elucidate the effects of defect disorder and *e-e* interaction on the spectral density of the defect states emerging in the Mott-Hubbard gap of doped transition-metal oxides, such as $Y_{1-x}Ca_xVO_3$. A soft gap of kinetic origin develops in the defect band and survives defect disorder for *e-e* interaction strengths comparable to the defect potential and hopping integral values above a doping dependent threshold; otherwise only a pseudogap persists. These two regimes naturally emerge in the statistical distribution of gaps among different defect realizations, which turns out to be of Weibull type. Its shape parameter k determines the exponent of the power-law dependence of the density of states at the chemical potential $(k-1)$ and hence distinguishes between the soft gap ($k \geq 2$) and the pseudogap ($k < 2$) regimes. Both k and the effective gap scale with the hopping integral and the *e-e* interaction in a wide doping range. The motion of doped holes is confined by the closest defect potential and the overall spin-orbital structure. Such a generic behavior leads to complex nonhydrogenlike defect states that tend to preserve the underlying *C*-type spin and *G*-type orbital order and can be detected and analyzed via scanning tunneling microscopy.

DOI: 10.1103/PhysRevLett.115.206403 PACS numbers: 71.10.Fd, 68.35.Dv, 71.55.-i, 75.25.Dk

Defects in semiconductors and insulators determine their transport properties and are responsible for their usefulness for electronics. The hopping between defect states depends on their relative energy and is largely a function of disorder. In the case of small hopping amplitudes, the long-range *e-e* interaction becomes extremely relevant as it modifies substantially the energy of defect states and their occupations. In a seminal work [1,2], it was shown that a soft gap develops in the density of states (DOS), $N(\omega) \propto |\omega|^{\kappa}$ with exponent $\kappa = d-1$ for system dimension $d = 2, 3$, in the classical Coulomb glass model: it is known as the Coulomb gap [3]. Further theoretical [4–6] and experimental [7] studies confirmed the remarkable success of the strong coupling approach for defects.

We consider defects in a quite different class of compounds: Mott insulators exhibiting a Mott-Hubbard (MH) gap due to short-range *e-e* interactions [8] that separates the lower Hubbard band (LHB) from the upper Hubbard band (UHB) [9]. Defects in Mott insulators feature many fascinating behaviors [10–16] and are usually thought to lead to only two alternatives: either the MH gap collapses or the defect states inside the gap undergo an Anderson transition, as proposed by Mott [17] for $La_{1-x}Sr_xVO_3$ and for the high-T_c cuprates. However, why the insulator-to-metal transition occurs in vanadates at much higher doping than in cuprates, although in both systems the MH bands do not disappear with metallization [18,19], is still not understood. Then, instead of from the Anderson-Hubbard model that features only short-range Hubbard-like interactions and one orbital flavor [20–24], we start from an extended Hubbard model with long-range *e-e* interactions, which allows us to study the effect of the self-consistent screening of defect potentials, and three orbital flavors. It provides a platform for describing the spin-orbital correlations of the perovskite vanadates, such as $Y_{1-x}Ca_xVO_3$, with active $\{yz, zx\}$ orbitals at $V^{3+}(xy)^1(yz/zx)^1$ ions, and coexisting *C*-type antiferromagnetic (*C*-AF) spin and *G*-type alternating orbital (*G*-AO) order [25], see Figs. 1(a) and 1(b).

The motion of a doped hole is bound to the charged Ca defect [Fig. 1(b)] and is further controlled by the underlying spin-orbital structure: it forms a localized spin-orbital polaron [26,27]. Figure 1(c) displays the associated defect states in the MH gap in the case of a periodic arrangement of defects or, equivalently, of a short-range defect potential [28], and it also reveals the multiplets in the UHB. Because of the *CG* spin-orbital order, holes tend to form dimer states on specific *c* bonds, the *active* bonds, which results in the formation of a kinetic gap, see Fig. 1(d). Our main goal is to understand whether this kinetic gap survives the potential fluctuations of random defects with long-range Coulomb potentials and which role the screening due to the t_{2g} electrons plays.

Crucial to our analysis are the electron-defect (V_{im}^{D}) and the *e-e* (V_{ij}) interactions, both screened by the background dielectric constant ϵ_c due to core electrons (no t_{2g} electrons),

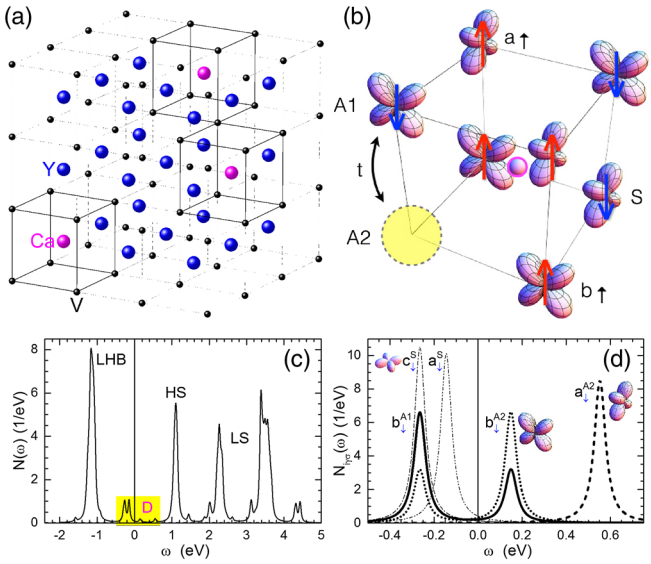

FIG. 1 (color online). (a) $Y_{1-x}Ca_xVO_3$ lattice with a random distribution of Ca defects. (b) A Ca defect in the center of a cube made of 8 V ions. The related hole (yellow circle) is confined to move (hopping t) along a vertical bond: the *active* $\langle A1, A2\rangle$ bond. The occupied a/b orbitals and spin states obey C-AF spin and G-AO order [19] on *spectator* (S) sites. (c) The LHB and the high-spin (HS) and low-spin (LS) states of the UHB for a periodic arrangement of defects and $x = 2\%$. The defect states D (yellow rectangle) are located within the MH gap for $V_D = 1.0$ eV and $t = 0.2$ eV. (d) The zoom of the defect states D uncovers the contributions of the *active* bond and *spectator* sites (heavy and thin lines) and the formation of the kinetic gap.

$$V_{im}^D = v(R_{im}), \quad V_{ij} = \eta v(r_{ij}), \quad v(r) = \frac{e^2}{\epsilon_c r}, \qquad (1)$$

where R_{im} and r_{ij} stand for the electronic distances between the V ion at site i and the Ca defect at site m and between two V ions at sites i and j, respectively. The typical binding energy of a hole is $V_D = V^D(d) \approx 1$ eV [19], where d is the distance between the defect and its closest V ions and $\epsilon_c \simeq 5$. A hole would propagate along the c axis at $V_D = 0$ [29], similar to an e_g hole in $Y_{2-x}Ca_xBaNiO_6$ [30].

The Hamiltonian of the doped $Y_{1-x}Ca_xVO_3$ reads as

$$\mathcal{H}_{t2g} = \sum_{im} V_{im}^D n_i + \sum_{i\neq j} V_{ij} n_i n_j + \mathcal{H}_{\rm CF} + \mathcal{H}_{\rm JT} - \sum_{\langle ij\rangle\sigma\alpha} t_{ij}^{\alpha}(d_{i\sigma\alpha}^{\dagger} d_{j\sigma\alpha} + \text{H.c.}) + \mathcal{H}_{\rm loc}(U, J_H), \qquad (2)$$

where $n_i = \sum_{\sigma\alpha} n_{i\sigma\alpha}$ and $n_{i\sigma\alpha} = d_{i\sigma\alpha}^{\dagger} d_{i\sigma\alpha}$, with orbital flavor $\alpha \in \{a, b, c\}$ standing for $a \equiv yz$, $b \equiv zx$, $c \equiv xy$. The first two terms in Eq. (2) basically resemble the Coulomb glass model [1,2] with site energies determined by the (random) positions of defects. The e-e interaction V_{ij} plays a major role in determining the occupation of these states as for $\eta = 1$ the combined defect-hole potential is dipolar [31], while for $\eta = 0$ it is monopolar. V_{ij} is also responsible for the additional screening involving the transitions between the Hubbard bands and the defect states. Further terms in the first line, $\mathcal{H}_{\rm CF} = -\Delta_c \sum_{i\sigma} n_{i\sigma c}$ and $\mathcal{H}_{\rm JT}$, denote the crystal-field and Jahn-Teller terms for the t_{2g} electrons [28]. A new dimension of the defect problem arises from the second line that includes the nearest-neighbor hopping (the symmetry of t_{2g} orbitals implies that t_{ij}^{α} is equal to t and different from 0 only for a bond $\langle ij\rangle$ direction different from α [32–34]), and the local Hubbard physics of the triply degenerate t_{2g} electrons, $\mathcal{H}_{\rm loc}(U, J_H)$ [35]. The local Coulomb interactions include intraorbital Hubbard U and Hund's exchange J_H expressed in the SU(2) invariant form [36]. They are responsible for the multiplets in the UHB for d-d charge excitations [Fig. 1(c)].

We solve the Hamiltonian Eq. (2) self-consistently employing the unrestricted Hartree-Fock (UHF) approximation [37]. There are two main advantages of the UHF approach we would like to emphasize: (i) UHF approximation reproduces the Hubbard bands and the multiplet splitting not only for undoped systems [37], but also in the presence of defects [27] and orbital polarization, and SU(2) rotation [28]; (ii) the spatial distribution and the occupation of each defect state depends on all other occupied states in the presence of disorder and long-range interactions [Eq. (1)]. As a matter of fact, UHF approximation solves this central and complex optimization problem in the most efficient way. The derivation of the UHF equations is standard; more details can be found, for instance, in Refs. [27,28]. We present results obtained for a cluster of $N_a = 8 \times 8 \times 8$ V ions with periodic boundary conditions, after averaging over $M = 100$ statistically different Ca defect realizations. We use the standard parameters for YVO_3, i.e., $U = 4.0$ eV, $J_H = 0.6$ eV, $\Delta_c = 0.1$ eV [28].

The $2_{\rm spin} \times 3_{\rm orbital} \times N_a$ UHF eigenvalues $\epsilon_{s,l}$ obtained for a given defect realization s yield the averaged DOS per V ion,

$$N(\omega) = \frac{1}{M}\sum_{s=1}^{M}\left[\frac{1}{N_a}\sum_{l=1}^{6N_a}\delta(\omega + \mu_s - \epsilon_{s,l})\right]. \qquad (3)$$

The Fermi energy μ_s not only separates the occupied from the unoccupied states in each defect realization s, but as well reflects, via the energy optimization, a repulsion between such states as in the Peierls effect [38]. Therefore, the average over different defect realizations calls for an overall alignment of the energy scales by means of the different μ_s.

Figure 2 displays the variation of the MH multiplets for different strengths of e-e interaction, encoded by the parameter η, for doping $x = 2\%$ of random Ca defects (i.e., for 10 defects) [cf. Figs. 1(c) and 1(d) for a periodic arrangement of defects]. The electronic states close to the

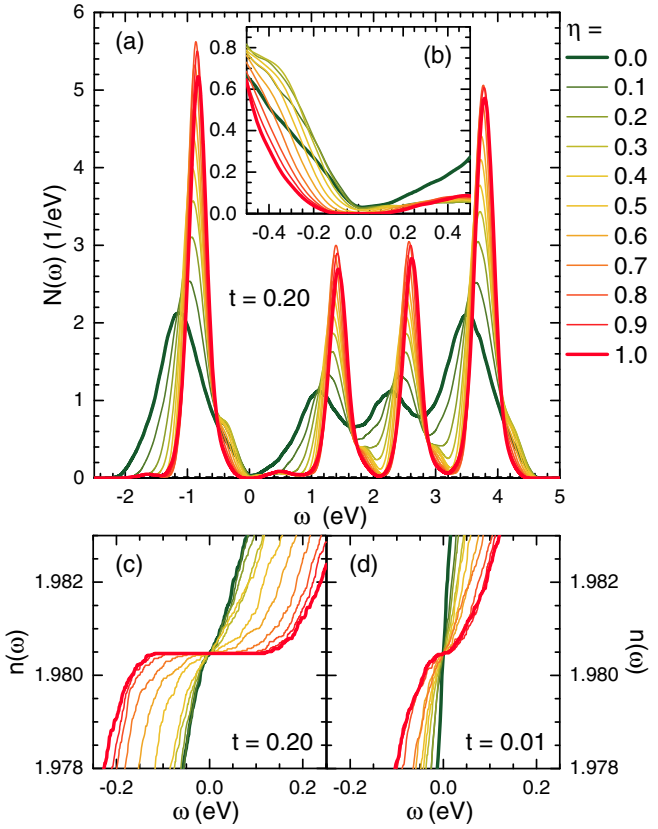

FIG. 2 (color online). (a) Density of states $N(\omega)$ averaged over $M = 100$ defect realizations for doping concentration $x = 2\%$, $t = 0.2$ eV, and for $\eta \in [0, 1]$. A Gaussian smearing of 0.03 eV has been used. Inset (b) shows a zoom of $N(\omega)$ in (a) close to the Fermi energy ($\omega = 0$). A zoom of the averaged integrated DOS $n(\omega)$ close to Fermi energy is shown for: (c) $t = 0.2$ eV, and (d) $t = 0.01$ eV.

defects are pushed by the potential V_D away from the LHB into the MH gap. However, the actual energy distribution of defect states is strongly dependent on the screening of the t_{2g} electrons via the e-e interaction and a soft gap gradually opens up in the DOS on increasing η. The Fig. 2(b) inset clearly shows the nonmonotonic variation of the defect states inside the MH gap on varying the screening. On the large energy scale, two important changes occur when η is varied. For $\eta = 0$, the defect potential is unscreened and the interaction with further randomly distributed defects broadens the Hubbard bands. For $\eta = 1$, the screening is instead complete: each defect forms an exciton with a doped hole and the resulting interaction between excitons is dipolar with a tremendous suppression of the effects of disorder and a dramatic narrowing of the Hubbard bands.

To analyze the behavior of the soft gap in $N(\omega)$ without suffering from the unavoidable smearing, we discuss next the averaged integrated DOS, $n(\omega) = \int_{-\infty}^{\omega} d\omega' N(\omega')$, in the vicinity of the Fermi energy and the related plateau [see Figs. 2(c) and 2(d)]. It is worth noting the following key features in $n(\omega)$: (i) there is an evident gap/plateau for $t = 0.2$ eV (being a typical value for cubic vanadates [32]) and $\eta = 1$, but not for small $t = 0.01$ eV, and (ii) on decreasing the screening $\eta \to 0$, the gap/plateau disappears even for $t = 0.2$ eV.

In order to establish the statistical behavior of $N(\omega)$ in the limit $M \to \infty$, we use that $N(\omega)$ is proportional to the probability distribution function $P^*(\omega)$ that a state in a generic defect realization has energy ω relative to its Fermi energy μ_s. Then, we find that a generic defect realization features a gap of size E with a probability governed by a Weibull probability distribution function,

$$P(E) = \theta(E-\zeta)\frac{k}{\lambda}\left(\frac{E-\zeta}{\lambda}\right)^{k-1} e^{-((E-\zeta)/\lambda)^k}, \qquad (4)$$

with shape parameter k, scale parameter λ, and location parameter ζ. Accordingly, if $\zeta = 0$, we have $P^*(\omega) = (k/\lambda^k)|\omega|^{k-1}$ and $N(\omega) \propto |\omega|^{k-1}$ both for $|\omega| \ll \lambda$, that is we have a soft gap for $k \geq 2$, a pseudogap for $1 < k < 2$ and no gap for $k = 1$. Instead, if $\zeta > 0$, we have $N(\omega) = 0$ for $|\omega| \leq \zeta$ and $N(\omega) \propto (|\omega| - \zeta)^{k-1}$ for $\zeta < |\omega| \ll \lambda$, that is we have a hard gap. Thus, $P(E)$ results in a robust scheme to determine the behavior of $N(\omega)$ close to the Fermi energy, that is the presence and type of gap in the system. The numerical data obtained for the gaps of M defect realizations for $t = 0.2\,(0.01)$ eV and $\eta = 0$ and 1 are compared in Figs. 3(a) and 3(b) to the corresponding

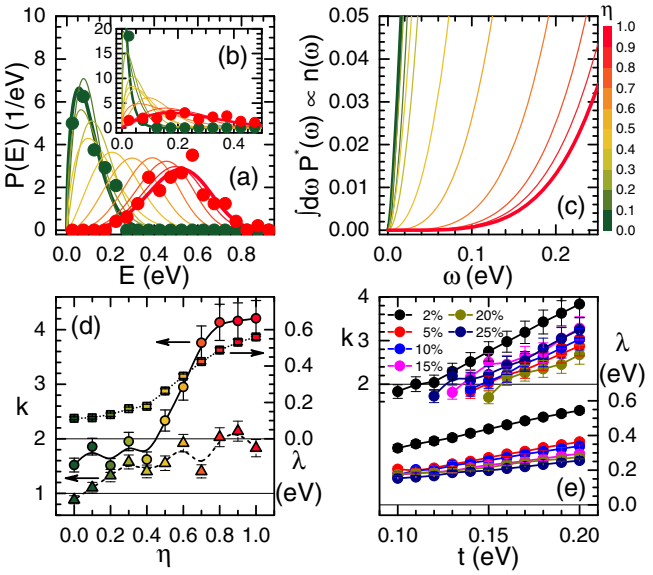

FIG. 3 (color online). (a) $P(E)$ for $t = 0.2$ eV and different values of η (colors as in Fig. 2). Lines are least-squares fits from Eq. (4) and dots are numerical data for $\eta = 0$ and 1 computed from the M defect realizations; inset (b) same as (a) but for $t = 0.01$ eV; (c) averaged integrated DOS $n(\omega)$ calculated from (4); (d) η dependence of k and λ for $t = 0.2$ eV (circles and squares, respectively) and for $t = 0.01$ eV (only k with triangles); (e) t dependence of k and λ for doping $x = 2\%$, 5%, 10%, 15%, 20%, and 25% at $\eta = 1$. Lines in (d) and (e) are guides to the eye.

statistical least-squares fits to $P(E)$. The fits are indeed excellent in all cases and give systematically $\zeta = 0$.

In Fig. 3(c), we report the $n(\omega)$ curves of Fig. 2(c) successfully reconstructed with the help of $P(E)$. The plateau/gap Δ present in Fig. 2(c) for $\eta \geq 0.5$ is due to the finiteness of M: its statistical value is $\Delta \doteq \lambda/\sqrt[k]{M}$ that vanishes for $M \to \infty$. Figures 3(d) and 3(e) summarize the dependence of k and λ on the e-e interaction strength η, and t, respectively. Both k and λ increase with increasing e-e interaction η, see Fig. 3(d). At $t = 0.2$ eV, for $\eta > 0.5$, we have $k > 2$ and, therefore, a soft gap. On the contrary, for $t = 0.01$ eV, $k < 2$ is found for all values of η: the e-e interaction *alone* is not sufficient to stabilize a gap and only a pseudogap persists. It is worth noting the almost linear increase of both k and λ with increasing t shown at $\eta = 1$ in Fig. 3(e), which justifies calling the soft gap a kinetic gap. We also observe a rather slow, but monotonic, decrease of λ on increasing the doping x. The most important feature is the nonuniversality of the exponent k that scales with both η and t, and is not simply given by the system dimensionality, in contrast to the Coulomb gap in disordered semiconductors [1,2].

The kinetic gap formation is triggered by the doped holes that do not form symmetric, hydrogenlike, orbitals around the defects. Instead, due to the interplay with the spin-orbital order, they form composite spin-orbital polarons that localize in a symmetry broken form on *active* bonds. Which of the four closest c bonds of a defect is chosen depends on the interactions with all other defects. To detect and analyze these complex defects, we study in the following the scanning tunneling microscopy (STM) patterns [39–42] that correspond here to the spatially resolved spin-orbital ($\sigma\alpha$) DOS integrated from the Fermi energy to the applied voltage V for a particular defect realization s, $\varrho_{\sigma\alpha}(x,y,z;V) = |\int_0^V d\omega \rho_{\sigma\alpha}(x,y,z;\omega+\mu_s)|$.

The integrated unoccupied density pattern summed over all spin-orbital degrees of freedom, $\sum_{\sigma\alpha}\varrho_{\sigma\alpha}(x,y,z;V)$, is shown in Fig. 4(a) for $V = 1.0$ eV. In the lower left corner, we recognize an unoccupied defect state (A) at coordinates $(x,y,z) = (2,1,z)$ with a finite hole density at vanadium sites $z = 1,2$ (on the *active* bond). The asymmetry relative to its closest Ca defect at (1.5,1.5,1.5) is evident. The degree of orbital polarization, i.e., increased weight at $z = 2$, is due to the other defects and the Jahn-Teller potential. Figure 4(b) shows the occupied density for $V = -0.7$ eV. Close to the same defect at (1.5,1.5,1.5), we see two occupied c bonds: one at (1,1,1) and (1,1,2) with two electrons per site (*spectator* sites), and another one at (2,1,1) and (2,1,2)—the *active* bond (A), with a single hole fluctuating in an asymmetric way along the bond parallel to the c axis. The defect (B) has its hole on a neighbor y plane and we see only *spectator* sites. (C) and (D) mark a pair of *active* bonds belonging to three V cubes hosting three defects. More defect states appear at $V = -0.8$ eV [Fig. 4(c)] that are not well separated from the LHB. Here

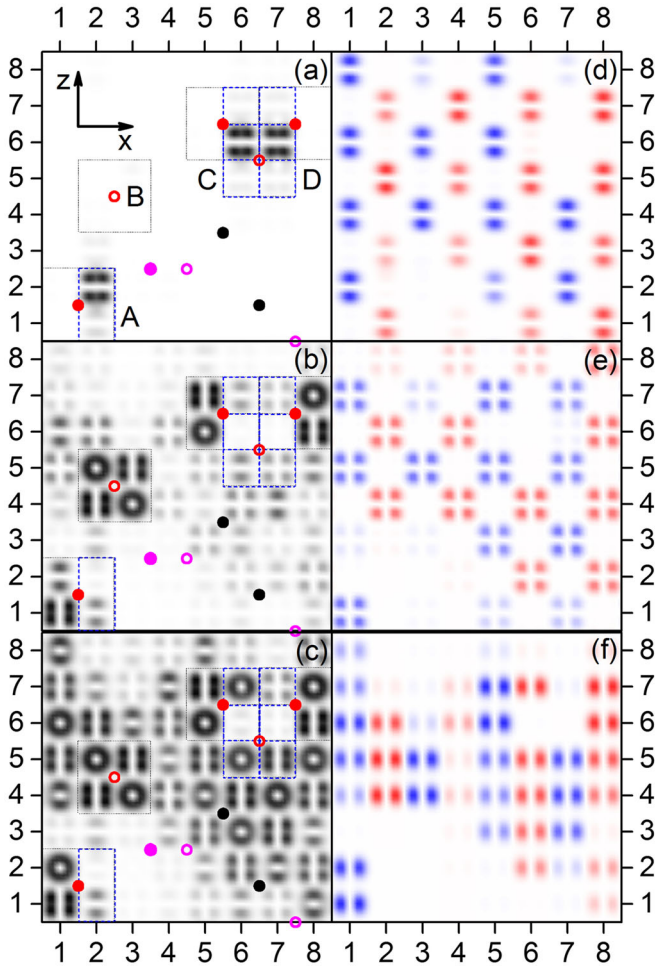

FIG. 4 (color online). Integrated electron/hole density $\varrho_{\sigma\alpha}(x,y,z;V)$ in the ac plane with $y = 1$ [V ions are at $(x,1,z)$ sites] for a typical defect realization at $x = 2\%$, $\eta = 1$, and $t = 0.2$ eV. The defects closest to the shown plane at $y = 1.5$ (0.5) are marked by red dots (circles), at $y = 2.5$ (7.5) by magenta dots (circles), and more distant ones by black dots. Faces of V cubes hosting a defect are indicated by thin gray dotted lines, while *active* bonds by thick blue dashed lines. Panel (a) shows the integrated unoccupied density at $V = 1.0$ eV, with defect features A, B, C, D discussed in the text; panels (b) and (c) show the integrated occupied density at: (b) $V = -0.7$ eV, (c) $V = -0.8$ eV. Right panels show the spin-orbital partial densities at $V = -0.8$ eV for: (d) $a = yz$, (e) $b = xz$, and (f) $c = xy$ orbitals. Red (blue) color for up (down) spin projections clearly shows C-AF order.

the complexity of the defect landscape is apparent as well as the interaction of the doped holes with the spin-orbital background.

The landscapes in Figs. 4(d)–4(f) represent the partly occupied spin-orbital densities $\varrho_{\sigma\alpha}(x,y,z;V)$ of *defect states* at $V = -0.8$ eV. The red (blue) stripe structure for up (down) spins reveals that both the underlying C-AF spin order and the G-AO order survive the doping by charge defects, in contrast to what happens in high-T_c cuprates where the spin order of the parent compound is

destroyed [43,44]. This supports the findings of Tokura's group that C-AF/G-AO order is preserved in various doped vanadate systems [19].

Summarizing, we have shown that charged defects in vanadates generate an intrinsic kinetic gap within the Mott-Hubbard gap that survives defect disorder for strong e-e interactions implying a strong dielectric screening. The kinetic gap transforms into a soft gap with power-law dependence: $N(\omega) \propto |\omega|^{k-1}$. We have established that the exponent k is nonuniversal and scales with both the kinetic scale t and the e-e interaction strength η. We suggest that an STM analysis can provide highly valuable microscopic information on the complex nonhydrogenlike states of doped holes, but this remains an experimental challenge.

We thank A. Rost and H. Shinaoka for insightful discussions. A. A. acknowledges the kind hospitality at Max-Planck-Institut für Festkörperforschung, Stuttgart. A. M. O. kindly acknowledges support by Narodowe Centrum Nauki (NCN, National Science Center) Project No. 2012/04/A/ST3/00331.

[1] A. L. Efros and B. I. Shklovskii, J. Phys. C **8**, L49 (1975).
[2] A. L. Efros, J. Phys. C **9**, 2021 (1976).
[3] M. Pollak, Philos. Mag. B **65**, 657 (1992).
[4] F. Epperlein, M. Schreiber, and T. Vojta, Phys. Rev. B **56**, 5890 (1997).
[5] M. Müller and L. B. Ioffe, Phys. Rev. Lett. **93**, 256403 (2004).
[6] A. L. Efros, B. Skinner, and B. I. Shklovskii, Phys. Rev. B **84**, 064204 (2011); B. Skinner, T. Chen, and B. I. Shklovskii, Phys. Rev. Lett. **109**, 176801 (2012).
[7] V. Yu. Butko, J. F. DiTusa, and P. W. Adams, Phys. Rev. Lett. **84**, 1543 (2000).
[8] M. Imada, A. Fujimori, and Y. Tokura, Rev. Mod. Phys. **70**, 1039 (1998).
[9] H. Eskes, M. B. J. Meinders, and G. A. Sawatzky, Phys. Rev. Lett. **67**, 1035 (1991); M. B. J. Meinders, H. Eskes, and G. A. Sawatzky, Phys. Rev. B **48**, 3916 (1993).
[10] W. Brzezicki, A. M. Oleś, and M. Cuoco, Phys. Rev. X **5**, 011037 (2015).
[11] T. Tanaka, M. Matsumoto, and S. Ishihara, Phys. Rev. Lett. **95**, 267204 (2005).
[12] K. W. Kim, J. S. Lee, T. W. Noh, S. R. Lee, and K. Char, Phys. Rev. B **71**, 125104 (2005).
[13] C. Şen, G. Alvarez, and E. Dagotto, Phys. Rev. Lett. **105**, 097203 (2010).
[14] J.-Q. Yan, J.-S. Zhou, J. G. Cheng, J. B. Goodenough, Y. Ren, A. Llobet, and R. J. McQueeney, Phys. Rev. B **84**, 214405 (2011).
[15] N. Pavlenko, T. Kopp, E. Y. Tsymbal, G. A. Sawatzky, and J. Mannhart, Phys. Rev. B **85**, 020407(R) (2012); N. Pavlenko, T. Kopp, E. Y. Tsymbal, J. Mannhart, and G. A. Sawatzky, *ibid.* **86**, 064431 (2012).
[16] H. O. Jeschke, J. Shen, and R. Valenti, New J. Phys. **17**, 023034 (2015).
[17] N. F. Mott, J. Phys. II (France) **50**, 2811 (1989).
[18] P. Abbamonte, A. Rusydi, S. Smadici, G. D. Gu, G. A. Sawatzky, and D. L. Feng, Nat. Phys. **1**, 155 (2005).
[19] J. Fujioka, S. Miyasaka, and Y. Tokura, Phys. Rev. B **77**, 144402 (2008).
[20] D. Belitz and T. R. Kirkpatrick, Rev. Mod. Phys. **66**, 261 (1994).
[21] H. Shinaoka and M. Imada, J. Phys. Soc. Jpn. **78**, 094708 (2009).
[22] V. Dobrosavljević and G. Kotliar, Phys. Rev. Lett. **78**, 3943 (1997); M. C. O. Aguiar, V. Dobrosavljević, E. Abrahams, and G. Kotliar, *ibid.* **102**, 156402 (2009).
[23] Y. Song, R. Wortis, and W. A. Atkinson, Phys. Rev. B **77**, 054202 (2008).
[24] M. Sawicki, D. Chiba, A. Korbecka, Y. Nishitani, J. A. Majewski, F. Matsukura, T. Dietl, and H. Ohno, Nat. Phys. **6**, 22 (2010); C. Śliwa and T. Dietl, Phys. Rev. B **83**, 245210 (2011).
[25] J. Fujioka, T. Yasue, S. Miyasaka, Y. Yamasaki, T. Arima, H. Sagayama, T. Inami, K. Ishii, and Y. Tokura, Phys. Rev. B **82**, 144425 (2010).
[26] K. Wohlfeld, A. M. Oleś, and P. Horsch, Phys. Rev. B **79**, 224433 (2009).
[27] P. Horsch and A. M. Oleś, Phys. Rev. B **84**, 064429 (2011).
[28] A. Avella, P. Horsch, and A. M. Oleś, Phys. Rev. B **87**, 045132 (2013).
[29] S. Ishihara, Phys. Rev. Lett. **94**, 156408 (2005).
[30] E. Dagotto, J. Riera, A. Sandvik, and A. Moreo, Phys. Rev. Lett. **76**, 1731 (1996).
[31] Except for the monopolar interaction with the closest defect.
[32] G. Khaliullin, P. Horsch, and A. M. Oleś, Phys. Rev. Lett. **86**, 3879 (2001); Phys. Rev. B **70**, 195103 (2004).
[33] A. B. Harris, T. Yildirim, A. Aharony, O. Entin-Wohlman, and I. Y. Korenblit, Phys. Rev. Lett. **91**, 087206 (2003).
[34] M. Daghofer, K. Wohlfeld, A. M. Oleś, E. Arrigoni, and P. Horsch, Phys. Rev. Lett. **100**, 066403 (2008); P. Wróbel and A. M. Oleś, *ibid.* **104**, 206401 (2010).
[35] M. Daghofer, A. Nicholson, A. Moreo, and E. Dagotto, Phys. Rev. B **81**, 014511 (2010).
[36] A. M. Oleś, Phys. Rev. B **28**, 327 (1983).
[37] T. Mizokawa and A. Fujimori, Phys. Rev. B **54**, 5368 (1996).
[38] P. Horsch and F. Mack, Eur. Phys. J. B **5**, 367 (1998).
[39] Ø. Fischer, M. Kugler, I. Maggio-Aprile, C. Berthod, and C. Renner, Rev. Mod. Phys. **79**, 353 (2007).
[40] J. I. Pascual, J. Gómez-Herrero, C. Rogero, A. M. Baró, D. Sánchez-Portal, E. Artacho, P. Ordejón, and J. M. Soler, Chem. Phys. Lett. **321**, 78 (2000).
[41] D. A. Muller, N. Nakagawa, A. Ohtomo, J. L. Grazul, and H. Y. Hwang, Nature (London) **430**, 657 (2004).
[42] M. J. Lawler, K. Fujita, J. Lee, A. R. Schmidt, Y. Kohsaka, C. K. Kim, H. Eisaki, S. Uchida, J. C. Davis, J. P. Sethna, and E.-A. Kim, Nature (London) **466**, 347 (2010).
[43] G. Khaliullin and P. Horsch, Phys. Rev. B **47**, 463 (1993).
[44] A. Avella, F. Mancini, and R. Münzner, Phys. Rev. B **63**, 245117 (2001).